Rajasegar, R.; Niki, Y.; Li, Z.; García-Oliver, JM.; Musculus, MPB. (2021). Influence of pilot-fuel mixing on the spatio-temporal progression of two-stage autoignition of diesel-sprays in low-reactivity ambient fuel-air mixture. Proceedings of the Combustion Institute. 38(4):5741-5750. https://doi.org/10.1016/j.proci.2020.11.005

Title: ***Influence of Pilot-Fuel Mixing on the Spatio-Temporal Progression of Two-Stage Autoignition of Diesel-Sprays in Low-Reactivity Ambient Fuel-Air Mixture***

Authors and Affiliations:

- **Rajavasanth Rajasegar:** Combustion Research Facility, Sandia National Laboratories, Livermore, CA, 94550, USA.
- **Yoichi Niki:** National Institute of Maritime, Port and Aviation Technology, Tokyo, 181-0004, Japan.
- **Zheming Li:** Combustion Research Facility, Sandia National Laboratories, Livermore, CA, 94550, USA.
- **Jose Maria Garcia Oliver:** CMT - Motores Térmicos, Universitat Politècnica de València, Valencia, 46022, Spain.
- **Mark P. B. Musculus:** Combustion Research Facility, Sandia National Laboratories, Livermore, CA, 94550, USA.

Colloquium: RECIPROCATING INTERNAL COMBUSTION ENGINES

Corresponding Author

- **Rajavasanth Rajasegar**

  Combustion Research Facility

  Sandia National Laboratories

  Livermore, CA, 94550, USA

  Phone: +1-925-294-6401

  E-mail: rrajase@sandia.gov

Influence of Pilot-Fuel Mixing on the Spatio-Temporal Progression of Two-Stage Autoignition of Diesel-Sprays in Low-Reactivity Ambient Fuel-Air Mixture

Rajavasanth Rajasegar[1], Yoichi Niki[2], Zheming Li[1], Jose Maria Garcia Oliver[3], Mark P. B. Musculus[1]

[1]*Combustion Research Facility, Sandia National Laboratories, Livermore, CA, 94550, USA*

[2]*National Institute of Maritime, Port and Aviation Technology, Tokyo, 181-0004, Japan*

[3]*Universitat Politècnica de València, Valencia, 46022, Spain*

Abstract

The spatial and temporal locations of autoignition for direct-injection compression-ignition engines depend on fuel chemistry, temperature, pressure, and mixing trajectories in the fuel jets. Dual-fuel systems can provide insight into both fuel-chemistry and physical effects by varying fuel reactivities and engine operating conditions. In this context, the spatial and temporal progression of two-stage autoignition of a diesel-fuel surrogate, *n*-heptane, in a lean-premixed charge of synthetic natural-gas (NG) and air is imaged in an optically accessible heavy-duty diesel engine. The lean-premixed charge of NG is prepared by fumigation upstream of the engine intake manifold. Optical diagnostics include high-speed (15kfps) cool-flame chemiluminescence-imaging as an indicator of low-temperature heat-release (LTHR) and OH* chemiluminescence-imaging as an indicator high-temperature heat-release (HTHR). NG prolongs the ignition delay of the pilot fuel and increases the combustion duration. Zero-dimensional chemical-kinetics simulations provide further understanding by replicating a Lagrangian perspective for mixtures evolving along streamlines originating either at the fuel nozzle or in the ambient gas, for which the pilot-fuel concentration is either decreasing or increasing, respectively. The zero-dimensional simulations predict that LTHR initiates most likely on the air streamlines before transitioning to HTHR, either on fuel-streamlines or on air-streamlines in regions of near-constant ϕ. Due to the relatively short pilot-fuel injection-durations, the transient increase in entrainment near the end of injection (entrainment

wave) is important for quickly creating auto-ignitable mixtures. To achieve desired combustion characteristics, e.g., multiple ignition-kernels and favorable combustion phasing and location (e.g., for reducing wall heat-transfer or optimizing charge stratification), adjusting injection parameters could tailor mixing trajectories to offset changes in fuel ignition chemistry.

Keywords:

Lean-premixed natural-gas combustion, diesel, two-stage autoignition chemical kinetics, cool-flame imaging, OH*chemiluminescence imaging

1. Introduction

Understanding and controlling the interplay between in-cylinder physical and chemical processes that govern the ignition and combustion characteristics that dictate operating limits, pollutant formation, and fuel-conversion efficiency, are critical to the design and operation of combustion systems for direct-injection compression-ignition engines. In this context, pilot-fuel-ignited lean-premixed combustion of natural gas (NG), where combustion is initiated by a short pilot-injection of high-reactivity diesel-type liquid fuel into a low-reactivity, fuel-lean, premixed NG charge has received increasing attention due to its potential for reduced soot, CO_2 and NO_x emissions, and diesel-like compression ratios and efficiencies [1,2].

In this ‘diesel-piloted dual-fuel (DPDF) combustion’ approach, autoignition of the pilot-fuel is complicated by multiple degrees of stratification: temperature (pilot-fuel vaporization-cooling), equivalence-ratio (partial mixing of pilot-fuel), and reactivity (local variations in the ratio of high-reactivity pilot-fuel to low-reactivity NG). Hence, the spatial and temporal locations of autoignition are governed by both physical effects of mixing of pilot-fuel with premixed-NG and chemical effects of two-stage autoignition in the local NG/pilot-fuel/air mixtures.

Conventional metal-engine experiments on DPDF combustion focused primarily on engine-

performance, combustion-stability, knock, and emissions have shown considerable increase in the ignition-delay (ID) of the pilot-fuel in the presence of NG [2-4]. High-sensitivity of ID to changes in premixed-NG concentration, leading to prolonged combustion duration, large cycle-to-cycle variations, combustion-instability, and tendency to misfire at low loads with shorter pilot-injection durations resulting in a poor thermal-efficiency with increased methane slip, i.e., unburned hydrocarbon emissions, have been reported [2,3]. Further, these problems cannot be solved by changing injection-timing [4], and though increasing the pilot-fuel mass can yield more complete combustion of premixed NG, soot and NO_x emissions tend to increase [2,3]. Previous numerical studies [5] and few optical diagnostic experiments have provided insight into the in-cylinder temporal and spatial progression of ignition-delay, combustion, and soot formation [6-9]. Given that fundamental studies on two-stage autoignition behavior of single fuels under diesel-engine conditions have pointed to the importance of mixing [10,11], it is likely that mixing effects will be critical for understanding NG effects these in-cylinder processes. Nevertheless, better understanding is needed on how increasing or decreasing concentration of diesel-type fuel following streamlines during mixing with a NG premixture affects autoignition.

The goal of this work is to improve the fundamental understanding of the interplay between the physical and chemical processes of mixing and autoignition, which is essential for combustion system design and model development, both for DPDF and for spray combustion in general. Here, imaging of the spatial and temporal progression of two-stage autoignition of the pilot-fuel in the presence of NG is correlated with zero-dimensional chemical-kinetics simulations. Due to the ignition-inhibiting effects of NG on *n*-heptane autoignition, mixing effects on the progression of first-stage and second-stage ignition are increasingly important as the main-chamber NG concentration is increased. Thus, manipulation of mixing characteristics can offset changes in ignition chemistry of high-reactivity sprays in low-reactivity charge-gas to control and achieve favorable ignition characteristics and desired combustion phasing and location, which can be valuable for combustion design.

2. Experimental and Simulation Set-ups

2.1. Optical Engine and Operating Conditions

Figure 1 shows an engine schematic with the diagnostics setup. Table 1 lists operating conditions with engine/injector specifications. The optical engine is a single-cylinder, extended-piston version of Cummins-N14, heavy-duty diesel with a quiescent (low swirl) combustion chamber [12]. A flat UV-grade fused-silica piston-crown window provides imaging access from below to the open, right-cylindrical bowl. A Delphi DFI-1.5 common-rail injector delivers consistent, short-duration, *n*-heptane pilot-fuel injections. A Clean-Air SP010 gas-injector fumigates synthetic NG using a perforated annular tube inserted into the intake-air pipe, 0.55m upstream of the intake port. The gas-injector location and long residence-time from injection to induction (4-5 cycles) yields a well-mixed NG-air charge.

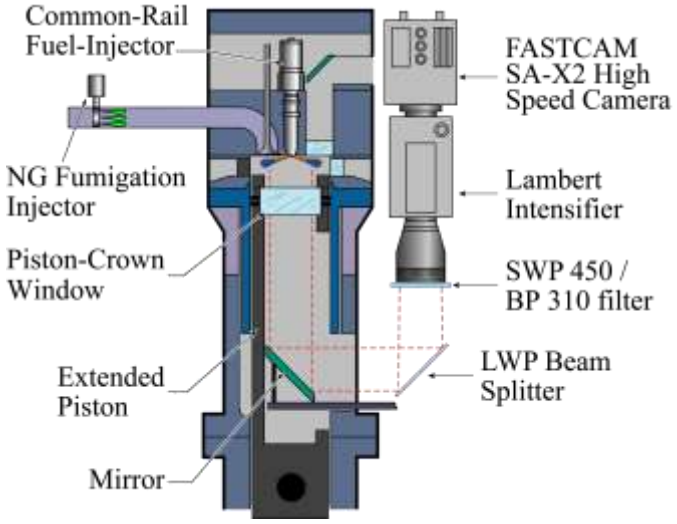

Figure 1. Optical engine and imaging setup.

The engine is operated at 1200 rpm in '9:1 skip-fire mode,' i.e., with pilot-fuel injections in one out of ten cycles. Two different pilot-fuel injections of equal pilot-fuel mass (11.2mg) are utilized, specified by fuel-rail pressure (FRP) / duration of solenoid energization (DSE): 400bar/760µs (low-pressure, long-duration pilot) and 800bar/500µs (high-pressure, short-duration pilot). The intake charge is either air (NG equivalence-ratio ϕ_{NG}=0) or premixed NG-air (ϕ_{NG}=0.5). From a practical perspective,

ϕ_{NG}=0.5 is interesting for low NOx, high efficiency, and manageable peak heat release, while short pilot-fuel injections maximize diesel-fuel replacement by NG. For the pilot-fuel injections, the start of solenoid energization (SSE) is held constant at 347 crank-angle degrees (CAD). Actual start of injection (SOI), end of injection (EOI), and duration of injection (DOI) were determined from infrared imaging (not shown here).

Engine and Injector Specifications	
Base engine	Cummins N-14, four-stroke diesel, 11.2 compression ratio
Engine geometry	13.97cm bore, 15.24cm stroke, 2.34L displacement,
Combustion chamber	Quiescent, direction injection, 0.5 swirl ratio
Bowl	Flat bottomed, 9.78cm wide, 1.55cm deep
Pilot-fuel injector	8-hole, 0.131mm orifice, 156º included angle, solenoid-actuated, Delphi DFI-1.5 common-rail
Pilot fuel	High-purity (>99%) *n*-heptane, 56 cetane number
NG injector	Fumigation, single-hole, solenoid-actuated, Clean Air SP010 gas-injector
NG fuel	Synthetic mixture: 95% CH_4, 4% C_2H_6 1% C_3H_8 by vol.
Operating Conditions	
Intake conditions	100ºC, 100kPa, 21% O_2
Engine speed	1200 rpm
NG injection parameters	1: No NG injection (ϕ_{NG}=0.0) 2: 7.5bar, SSE: 40CAD, DSE: 12.45ms (ϕ_{NG}=0.5)
Pilot-fuel injection parameters	A: SSE: 347CAD, FRP: 400bar, DSE: 760µs, 11.5mg SOI: 349.75CAD, EOI: 356CAD, DOI: 868µs B: SSE: 347CAD, FRP: 800bar, DSE: 500µs, 11.5mg SOI: 349.5CAD, EOI: 354CAD, DOI: 625µs
SOI charge conditions	ϕ_{NG}=0.0 T=871.4K, P=21.75bar ϕ_{NG}=0.5 T=849.1K, P=21.75bar
TDC charge conditions	ϕ_{NG}=0.0 T=896.4K, P=24.25bar ϕ_{NG}=0.5 T=872.1K, P=24.25bar

Table 1. Engine specifications and operating conditions.

2.2. Diagnostics

Apparent heat-release rate (AHRR) is calculated from cylinder pressure measured every 0.25º crank angle using a piezoelectric pressure-transducer (AVL-QC34D). Cylinder-pressure data are smoothed using a Fourier-series low-pass filter with a Gaussian roll-off function (transmission of 100% at 0-800Hz, 1% at 3360Hz) to remove acoustic ringing while retaining important AHRR features [13]. Crank-angle resolved, non-sequential, first-stage, cool-flame chemiluminescence (415-440nm band-pass filter, 105mm glass-lens at f/2.5) [14] and second-stage, high-temperature, filtered-OH* chemiluminescence (10nm wide, 310nm band-pass filter, 105mm UV-lens at f/8-f/11) [14] are captured using a high-speed camera (Photron FASTCAM-SAX-2) coupled to a high-speed intensifier (Lambert Hi-CATT-S-20). Since the filter and glass-lens setup for cool-flame chemiluminescence imaging successfully rejects OH* chemiluminescence, and as images are acquired before soot formation, the recorded intensity is most likely dominated by chemiluminescence from HCHO*, HCO*, CH*, CO_2*, and/or broadband emission from the CO continuum [15]. These two filtering setups track the spatial and temporal evolution of cool-flame and hydroxyl radical OH* in two-stage-autoignition of *n*-heptane-NG mixtures. Cool-flame emission occurs during low-temperature heat-release (LTHR), while OH* concentrations are orders of magnitude larger during high-temperature heat-release (HTHR) than in LTHR [14].

2.3. Chemical-Kinetics Simulations

To complement the experimental data, the chemical-kinetics of autoignition in *n*-heptane-NG mixtures are simulated using the Ansys CHEMKIN-Pro package with the Lawrence-Livermore detailed *n*-heptane mechanism version 3.1 [16], which also includes chemistry for methane, ethane, and propane of our synthetic NG. These simulations are not intended to replicate the experimental data, nor are they appropriate for high-fidelity predictions. Rather, they are intended for limiting-case analysis to develop understanding from a simplified mean-flow Lagrangian perspective. The goal is to gain insight into the interplay between the physical and chemical processes of mixing and two-stage autoignition from a series

of simplified canonical scenarios: a zero-dimensional, closed homogenous-reactor (CHR) model to isolate the chemical effects of premixed NG on *n*-heptane autoignition, and a perfectly-stirred reactor (PSR) model to add simple mixing effects.

The simple CHR model is utilized to decouple chemistry from other simultaneous (mixing) processes, providing straightforward parametric understanding of mixture-state effects on ignition. The CHR is initialized at the in-cylinder pressure and temperature at the pilot-fuel SOI, accounting for fuel-vaporization-cooling and adiabatic compression of various *n*-heptane-NG-air mixture compositions that may exist within the pilot-fuel jet. IDs for first-stage low-temperature (LTID) and second-stage high-temperature (HTID) ignition are computed based on the relevant inflection point in the temperature profile. The CHR model only accounts for the chemical induction portion of in-cylinder processes, as the reactor does not interact with other local mixtures.

While spatially-resolved combustion models [10,17,18] that capture both fluid-mechanic and chemical processes could be used in conjunction with the experiments, we opted for the PSR-model [19] as a simple first-order representation of the interplay between pilot fuel-jet entrainment mixing and auto-ignition chemistry from a Lagrangian perspective along ensemble-averaged streamlines originating either in the diesel injector-nozzle or the entrained ambient-gas (Figure 4, left-panel). The simplified PSR model accounts for accumulation of reaction products and transport of fresh reactants, but it does not include turbulence-chemistry interaction or transport of reaction products. One PSR is initialized with pure *n*-heptane at the SOI in-cylinder pressure and 373 K with an inflow of premixed-NG-air at the SOI temperature, which represents ‘fuel’ streamlines originating from the injector-nozzle. Fuel streamlines experience a decreasing *n*-heptane concentration, which is replicated trendwise by this PSR setup. A second PSR is initialized with a pure in-cylinder NG-air charge with an inflow of *n*-heptane fuel at the vaporized fuel-temperature, which represents ‘air’ streamlines originating in the air-NG mixture that is entrained into the pilot jet. For this air-streamline PSR, the initial temperature of *n*-heptane is intentionally

lowered to 130K to account for charge-cooling in these single-phase simulations by matching the adiabatic-mixing temperatures that are realized later, after fuel vaporization, as verified by non-reactive simulations for $0.1<\phi_{pilot}<5$. To explore mixing-rate effects on LTID and HTID, the characteristic 1/e PSR-mixing-time τ (equal to the mean residence-time with no diffusion) is varied parametrically.

3. Results and Discussion

3.1. Image Processing

Quantitative and qualitative information about the spatial and temporal progress of autoignition and subsequent combustion of pilot-fuel injections into premixed NG-air from hundreds of non-sequential, high-speed, cool-flame and OH* chemiluminescence images are distilled into one single plot for each condition. Figure 2 is a compilation for four different conditions, as described in the following paragraphs.

First, the inset in Figure 2.i shows sector masks for processing the raw cool-flame or OH* chemiluminescence images, like those at the bottom of Figure 2.i, false colored in blue and red scales, respectively. Chemiluminescence intensities are averaged along the azimuthal direction within these sector masks at various distances downstream of the injector (indicated by colored circles in inset of Figure 2.i). These intensities are then normalized to the maximum intensity in the corresponding set of images for each of the four operating conditions in Figure 2. This normalized, azimuthally-averaged intensity (see adjoining color-bars) is plotted as a function of axial distance from the injector and CAD as filled-color contour plots (blue for cool-flame; red for OH* chemiluminescence) for each operating condition. Each vertical slice of the contour plot represents the variation radially outward from the injector of normalized azimuthally-averaged chemiluminescence-intensity, extracted from a single snapshot at a given CAD.

The corresponding AHRR (shown in green) for each operating condition is superimposed on the contour plot with key combustion events demarcated. The two series of images below each contour plot are snapshots of cool-flame and OH* chemiluminescence-images at key timings during the LTHR and

HTHR. The acquisition CAD and ordered indicators 1-5, A-E are affixed on upper-left and right corner respectively, with the same labels on the contour plots. For all test cases explored here, the timing of peak AHRR (both LTHR and HTHR) correlates well with the corresponding maximum chemiluminescence-intensity, so it is reasonable to consider cool-flame and OH* chemiluminescence images as indictors of LTHR and HTHR, respectively.

3.2. Effect of Natural-Gas on Pilot-Fuel Autoignition and Combustion Characteristics

Table 2 summarizes test-conditions and number of ignition kernels observed across all 30 fired cycles. Without premixed NG (cases:i-ii), all eight fuel jets ignite consistently for both pilot-fuel-injection conditions studied (400bar/760μs and 800bar/500μs). Though addition of NG (ϕ_{NG}=0.5, cases:iii-iv) changes ignition behavior (fewer ignition-kernels), in general, its effect is significantly more pronounced on the 800bar/500μs short-duration pilot (3/30 cycles misfire, 25/30 cycles with 1-3 ignition-kernels, none with all eight jets igniting) despite both pilot injections containing equal mass of *n*-heptane (11.2mg). The stark dissimilarity in the macro-ignition characteristics with or without premixed NG among two-similarly behaving pure *n*-heptane pilot-fuel injections implies that the interplay between physical and chemical processes of mixing and autoignition govern DPDF combustion.

Test-Conditions				
Case	I	ii	iii	iv
FRP (bar)	400	800	400	800
DSE (μs)	760	500	760	500
Pre-pilot NG EQR ϕ_{NG}	0	0	0.5	0.5
Ignition-kernel counts across 30 cycles				
0 kernel - misfire, no HTHR	0	0	0	3
1 to 3 kernels	0	0	0	**25**
4 to 7 kernels	0	0	9	2
8 kernels	**30**	**30**	**21**	0

Table 2. Summary of test-conditions along with ignition-kernel distribution.

3.2.1. *n*-heptane-only combustion

For conditions without any premixed-NG, based on Figure 2.i (400bar/760µs) and Figure 2.ii (800bar/500µs), several distinctions can be made between the two pilot-injection cases. The 800bar/500µs pilot has a shorter LTID of 6.7ºCA (8.5ºCA for 400bar/760µs-pilot) which is likely due to the earlier occurrence of a stronger "EOI entrainment-wave" [20], which causes a transient three-fold increase in mixing [20,21], creating auto-ignitable mixtures more quickly, resulting in shorter LTIDs [10]. However, despite the shorter LTID, the 800bar/500µs-pilot undergoes a relatively long LTID-to-HTID dwell of 5.3ºCA (3.8ºCA for 400bar/760µs-pilot) before the onset of HTHR. This results in similar HTID for both cases (~12ºCA). Furthermore, the 400bar/760µs-pilot has more rapid combustion, with a peak-AHRR of 95J/ºCA and 10ºCA combustion duration compared to 38J/ºCA and 14.5ºCA for the 800bar/500µs-pilot, caused most likely by the increased formation of kinetically slower fuel-lean mixtures due to over-mixing in the latter case.

The blue contour plot and snapshots of cool-flame chemiluminescence (blue) in both Figure 2.i and Figure 2.ii show similar characteristics: LTHR-reactions originate close to the injector (image:1, ~20mm downstream), proceed and reach the bowl-wall (image:3), which is then followed by the appearance of multiple hot-spots (regions of saturation) which indicate transition to HTHR. Also, consistent with increased mixing induced by the EOI entrainment-wave that creates fuel-lean regions near the injector [20] (i.e., faster leaning-out of mixture in the pilot-jet wake region), LTHR reactions proceed upstream toward the injector (image:2) as hotter gases there achieve low-temperature autoignition sooner, even though they are fuel lean [10]. Further, the contour plot and snapshots (images:3-5) clearly capture the period of increased dwell (reduced AHRR: decreasing chemiluminescence-intensities) for the 800bar/500µs-pilot. Finally, the transition to HTHR (image:5) occurs closer to the bowl-wall (~45mm

downstream of the injector) for the 800bar/500µs-pilot than for the 400bar/760µs-pilot (~35mm downstream). Indeed, the temporal and spatial locations of local hot-spots in the cool-flame chemiluminescence (image:5) coincide well (temporally within ~1CAD, spatially within ~5mm axially) with the first-detectable occurrence (SNR>3) of OH* chemiluminescence (image:A), though the two imaging-datasets are from two separate cycles from separate engine-runs.

The contour plot and snapshots of OH* chemiluminescence in Figure 2.i and Figure 2.ii show similar features during the early and late stages of HTHR. HTHR initiates close to the bowl-wall for one or a few pilot-fuel jets almost simultaneously (image:A) and then rapidly appears (within ~1ºCA) in all eight jets (image:B) which is followed by a rapid progression of sequential autoignition (images:C-E). However, with the 800bar/500µs-pilot, OH* chemiluminescence intensities are localized to the outer 50% of the combustion-chamber bore, while OH* chemiluminescence tends to proceed farther upstream (images:B-C), ~20mm downstream of the injector, for the 400bar/760µs-pilot, consistent with a weaker and later entrainment wave due to its lower FRP and longer DOI.

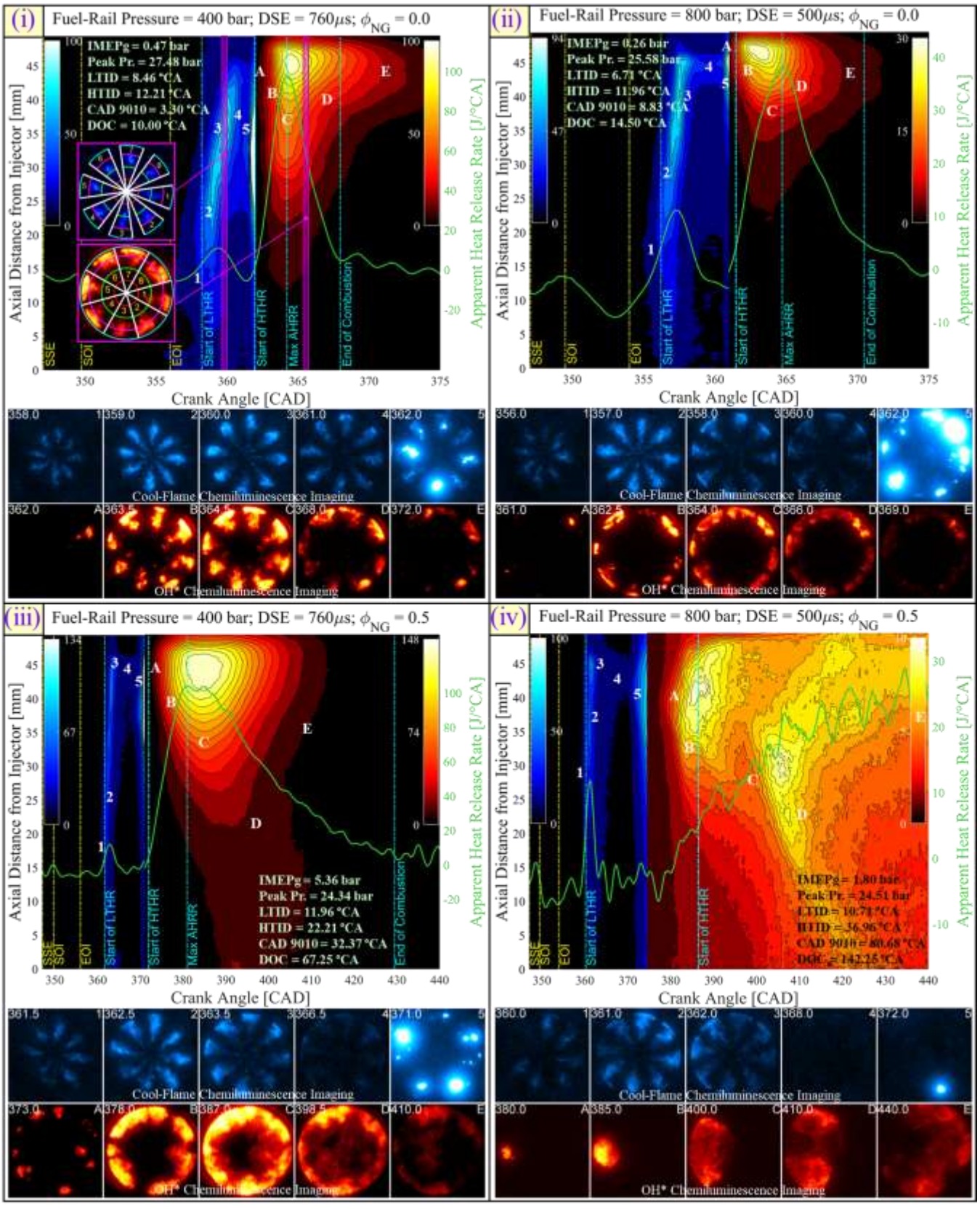
(i)
Fuel-Rail Pressure = 400 bar; DSE = 760μs; ϕNG = 0.0
IMEPg = 0.47 bar
Peak Pr. = 27.48 bar
LTID = 8.46 °CA
HTID = 12.21 °CA
CAD 9010 = 3.30 °CA
DOC = 10.00 °CA
(ii)
Fuel-Rail Pressure = 800 bar; DSE = 500μs; ϕNG = 0.0
IMEPg = 0.26 bar
Peak Pr. = 25.58 bar
LTID = 6.71 °CA
HTID = 11.96 °CA
CAD 9010 = 8.83 °CA
DOC = 14.50 °CA
(iii)
Fuel-Rail Pressure = 400 bar; DSE = 760μs; ϕNG = 0.5
IMEPg = 5.36 bar
Peak Pr. = 24.34 bar
LTID = 11.96 °CA
HTID = 22.21 °CA
CAD 9010 = 32.37 °CA
DOC = 67.25 °CA
(iv)
Fuel-Rail Pressure = 800 bar; DSE = 500μs; ϕNG = 0.5
IMEPg = 1.80 bar
Peak Pr. = 24.51 bar
LTID = 10.71 °CA
HTID = 36.96 °CA
CAD 9010 = 80.68 °CA
DOC = 142.25 °CA
Axial Distance from Injector [mm]
Crank Angle [CAD]
Apparent Heat Release Rate [J/°CA]
SSE
SOI
EOI
Start of LTHR
Start of HTHR
Max AHRR
End of Combustion
Cool-Flame Chemiluminescence Imaging
OH* Chemiluminescence Imaging

Figure 2. Imaging summaries for four operating conditions as indicated at the top of each quadrant. Color-contours in each quadrant are normalized, azimuthally-averaged cool-flame (shown in blue) and OH (shown in red) chemiluminescence-imaging intensities, superimposed with AHRR (shown in green) with key combustion events demarcated. Inset of (i), shows the azimuthal sector-masks for image analysis. Below each color-contour is a series of cool-flame and OH* images at key timings during LTHR and HTHR. Acquisition CAD is in the upper-left of each image, and image labels (1-5 and A-E) correspond to similar labels on the contour plots.*

3.2.2. *n*-heptane combustion with premixed-NG-air

Figure 2.iii (400bar/760µs/ϕ_{NG}=0.5) and Figure 2.iv (800bar/500µs/ϕ_{NG}=0.5) detail the effect of NG on two-stage autoignition of *n*-heptane for representative cycles based of the most populous ignition kernel type as listed in in Table 2. For both cases, adding NG increases the LTID (~50% increase to 12.0ºCA for 400bar/760µs-pilot; to 10.7ºCA for 800bar/500µs-pilot). However, the combination of early onset of the EOI entrainment-wave and the ignition-inhibition effect of NG are stronger for the 800bar/500µs-pilot, increasing its dwell period much more (5-fold increase to 26.25ºCA) than for the 400bar/760µs-pilot (10.3ºCA dwell), and further delaying the start of HTHR. The 800bar/500µs-pilot also exhibits higher cycle-to-cycle variability (Table 2) and longer burn-duration, resulting in lower closed-cycle efficiency due to reduced expansion ratio. The increased ID and variability are predominantly attributed to the ignition-inhibition effect of NG on pilot-fuel autoignition-chemistry and mixing effects related to injection pressure and increased mixing after EOI. To lesser degrees, changes in compressed-gas temperature at SOI due to variation in mixture specific-heat ratio and lower [O_2] due to dilution of air by NG [7] also have smaller effects. Notably, the peak-AHRR is unaffected by premixed NG despite the ~10-fold increase in IMEPg.

The contour plots and snapshots of cool-flame and OH* chemiluminescence provide additional

insight. Despite changes in temporal-progression, i.e., increased LTID (image:1), dwell (images:3-5) and HTID (images:5, A), the spatial-progression of two-stage autoignition of the 400bar/760μs-pilot with NG (Figure 2.iii) remains similar to without NG (Figure 2.i). The major differences are that LTHR originates farther downstream of the injector (~35mm downstream in image:1 of Figure 2.iii), cool-flame and OH* chemiluminescence-intensities are ~30% higher (compare maximum-scale of color-bars), and OH* chemiluminescence-contours extend closer to the injector. The images show a more distributed HTHR that is not confined to the pilot-jet boundary due to the availability of premixed NG-air capable of sustaining turbulent-flame propagation and/or sequential autoignition outside the jets (images:B-E). However, the temporal and spatial progression for the 800bar/500μs-pilot is markedly different in multiple aspects with (Figure 2.ii) and without (Figure 2.iv) NG. Due to a prolonged dwell-period (images:3-5) of reduced AHRR following LTHR, the probability of all pilot jets transitioning into second-stage autoignition is greatly decreased. For the representative cycle chosen, a single hot-spot after first-stage autoignition (image:5, Figure 2.iv) initiates HTHR reactions (image:A), followed by an apparent flame-front, slowly propagating through the cylinder well into the expansion stroke (gradual rise in AHRR with a long tail).

3.3. Chemical-Kinetics Simulations

Time-resolved simulated temperature-profiles from the CHR model exhibit typical two-stage-autoignition behavior characteristic of long-chain hydrocarbons like *n*-heptane, either with or without NG. Figure 3 shows the calculated LTID and HTID for different *n*-heptane-NG-air mixture compositions, accounting for fuel-vaporization cooling, which encompass the experimentally measured values despite the simplistic approach (i.e., no-mixing during reaction) of the CHR model. LTHR is favored by fuel-lean mixtures that are hotter (ϕ_{pilot}~0.5) [10], while the shortest HTID mixtures are the slightly fuel-rich most-reactive mixture fraction [22] (ϕ_{pilot}~1.1) [7,10]. The CHR model shows NG increasingly inhibits the autoignition chemistry of the *n*-heptane pilot-fuel, as indicated by the increasing IDs and slight shifts

in the shortest LTID and HTID toward progressively richer mixtures. This is likely due in part to reduced $[O_2]$, increased mixture thermal-capacity, and NG scavenging more radicals as ϕ_{NG} increases. Notably, the ID increases measured and calculated here with NG are more pronounced than established empirical relations for ignition during injection ($ID \sim [O_2]^{-1}$) [23], indicating that the kinetic effect of NG on *n*-heptane autoignition chemistry is more likely to be dominant than thermo-physical property effects.

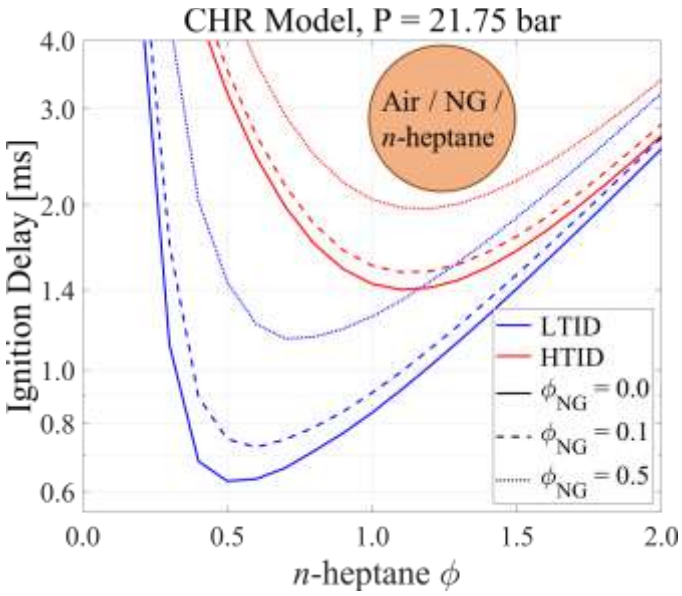

Figure 3. Predicted LTID and HTID from chemical-kinetics simulations using CHR model.

Although CHR-model predictions provide some insight into static mixture and chemical effects on ignition, they do not include dynamic mixing effects with chemistry occurring simultaneously with mixing, and hence IDs are much shorter than the experimental data, and they do not provide insight into mixing effects for different FRPs tested here. Additionally, with short pilot-injections, *n*-heptane mixtures in the CHR simulations are fuel-rich only for a short time such that they do not proceed to autoignition before becoming fuel-lean and even slower to autoignite. To explore dynamic mixing effects, PSR models are constructed to mimic Lagrangian perspectives of fuel and air-streamlines, as described in section 2.3. Notional temporal-distributions of equivalence ratio in the pilot jet under *non-reactive conditions* along the streamlines are shown in Figure 4 (left-panel). For fuel streamlines, the PSR is constructed with an

initial fuel mass that is progressively diluted with air, and hence the time-dependent equivalence-ratio decreases as ambient mass is incorporated into the initial *n*-heptane. From a Lagrangian perspective for a steady injection, this evolution scales approximately as the inverse of the axial distance from the injector orifice, and consequently with the inverse of the square root of time [24]. For air streamlines, the PSR starts with an initial ambient-gas mass that is fed with an evolving fuel stream. In this case, equivalence ratio first increases as the air streamline enters the jet, and later decreases as the overall jet leans out as it continues to penetrate. The bottom-middle and bottom-right panels show the evolution of the PSR instantaneous n-heptane-to-oxygen equivalence ratio for reacting cases, where consumption of *n*-heptane decreases the equivalence ratio at the two ignition stages. Note that for air streamlines, the equivalence ratio increases again well after ignition due to continued mixing with the fuel stream, though this late mixing is not relevant for the ignition analysis employed here. The simulations use a characteristic PSR mixing-time of τ=9.5ms for the air streamline, which yields comparable experimental, CHR-model, and PSR-model LTIDs (~1ms for ϕ_{pilot}~0.5) and HTIDs (~1.7ms for ϕ_{pilot}~1.1). For the fuel streamline, τ=1.9ms is the minimum τ to achieve two-stage autoignition in-line with experimental/CHR-model IDs, and also yields a similar equivalence-ratio history as predicted by a simple 1-D jet model [20]. Because the air streamlines asymptote to an unrealistically rich final state (pure fuel), they must use an artificially long τ. For τ=9.5ms, the air-streamline-based PSR-model (middle panel), predicts longer LTID from ϕ_{NG}=0 to ϕ_{NG}=0.1, consistent with experiments, but decreasing dwell-times between LTHR and HTHR, inconsistent with experiments. At ϕ_{NG}=0.5, no ignition occurs, also inconsistent with experiments. Increasing τ to 11.3ms yields ignition for the latter ϕ_{NG}, but the dwell between LTHR and HTHR is nearly zero.

By contrast, the fuel-streamline-based PSR-model (right panel), predicts longer LTIDs and increasing dwell times with increasing ϕ_{NG}, consistent with experiments. However, at ϕ_{NG}=0.5, only first-stage autoignition occurs for τ=1.9ms. If τ is increased to 2.4ms, two-stage auto-ignition is achieved, but

very late compared to experiments. Despite the shortcomings of the simplified PSR-models, they both exhibit increased sensitivity of two-stage auto-ignition to mixing rates with NG [7], i.e., increasing the characteristic mixing time (slower mixing) promotes autoignition of the pilot-fuel in premixed NG-air.

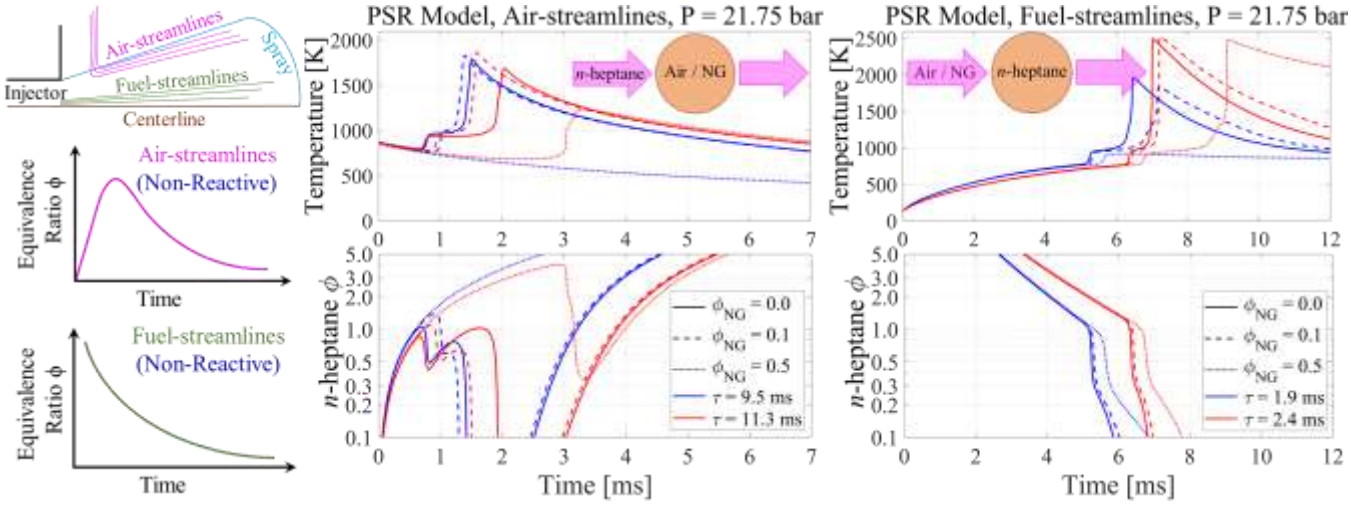

Figure 4. Left: Lagrangian perspective of fuel and air streamlines along with expected temporal distribution of equivalence ratio in the pilot-jet. Middle and Right: Predicted temperature (top) and equivalence-ratio profiles (bottom) from chemical-kinetics simulations using PSR model of air and fuel streamline respectively for varying ϕ_{NG} and characteristic mixing-time.

Based on the trends of LTID initially increasing with ϕ_{NG} for the air-streamline PSR and the CHR, which is consistent with experimental data, LTHR may initiate on air-streamlines either when ϕ is increasing or is nearly constant (c.f., Figure 4, left), consistent with LTHR initiating in the radial periphery of the pilot-jet [10,11]. For HTID, only the fuel-streamline PSR and CHR predict the observed trend of increasing HTID with ϕ_{NG}, so HTHR may initiate on fuel streamlines or in regions of air streamlines where ϕ remains constant. The interaction between local mixtures, e.g., complex dynamics of the "cool-flame wave" that links LTHR and HTHR [10,11], may be the mechanism that affects the transition between streamlines. Also, as the most-reactive mixture shifts to richer mixtures with NG, the relative location of the autoignition site on the streamlines may be relocated with longer HTID at faster mixing-rates/shorter

mixing-times. The characteristic mixing-time should scale as the inverse square-root of fuel-injection pressure [25], which is consistent with the shorter HTID and combustion duration of the lower-pressure, long-duration pilot injection into premixed NG-air.

4. Conclusions

Processes governing the spatial and temporal progression of two-stage autoignition of *n*-heptane in a lean-premixed charge of synthetic NG and air were investigated in an optically accessible heavy-duty diesel-engine using cool-flame and OH* chemiluminescence imaging. Interpretations of experimental observations were aided by zero-dimensional chemical-kinetics simulations using CHR and PSR models. The chemical-inhibition effect of NG prolongs LTID and HTID of the pilot-fuel. The EOI entrainment-wave-induced transient mixing-enhancement is earlier and stronger for the 800bar/500μs-pilot than for the 400/760μs-pilot, so it has hotter, more fuel-lean mixtures for which LTID is shorter but HTID is longer, irrespective of ϕ_{NG}. With NG, this causes a later onset and reduction in the number of ignition kernels, followed by slower apparent flame-propagation, resulting in longer combustion-durations. The PSR models predict LTHR initiates most likely on the air streamlines before transitioning to HTHR, either on fuel streamlines or on air streamlines in regions of near-constant ϕ, as predicted by the CHR model. Also, IDs are shorter at slower mixing rates in the presence of NG. The factor of 1.4 slower mixing rate of the 400bar/760μs-pilot results in earlier ignition with more kernels and shorter combustion-phasing. Thus, it should be possible to manipulate mixing characteristics by changing the pilot-fuel injection-parameters (e.g., FRP/DSE) to offset changes in ignition chemistry with NG to achieve desired ignition-characteristics and combustion-phasing and location, which would be a valuable tool for combustion design to improve fuel efficiency or reduce noise or perhaps even reduce heat-transfer losses by locating early combustion away from in-cylinder walls.

Acknowledgements

Support for this research at the Combustion Research Facility, Sandia National Laboratories,

Livermore, CA, was provided by the U.S. Department of Energy (DOE), Office of Energy Efficiency and Renewable Energy. Sandia is a multi-mission laboratory operated by National Technology and Engineering Solutions of Sandia, LLC., a wholly owned subsidiary of Honeywell International, Inc., for the U.S. DOE's National Nuclear Security Administration under contract DE-NA0003525.

References

1. G.A. Karim, Combustion in gas fueled compression: Ignition engines of the dual fuel type, J. Eng. Gas Turbines Power 125 (3) (2003) 827-836.
2. L. Wei, P. Geng, A review on natural gas/diesel dual fuel combustion, emissions and performance, Fuel Process. Tech. 142 (2016) 264-278.
3. J. Liu, F. Yang, H. Wang, M. Ouyang, S. Hao, Effects of pilot fuel quantity on the emissions characteristics of a CNG/diesel dual fuel engine with optimized pilot injection timing, Appl. Energy 110 (2013) 201-206.
4. R.M. Hanson, S.L. Kokjohn, D.A. Splitter, R.D. Reitz, An experimental investigation of fuel reactivity controlled PCCI combustion in a Heavy-Duty Engine, SAE Int. J. Engines 3 (1) (2010) 700-716.
5. E. Demosthenous, E. Mastorakos, R.S. Cant, Direct Numerical Simulations of Dual-Fuel Non-Premixed Autoignition, Comb. Sci. Tech. 188 (4-5) (2016) 542- 555.
6. S. Schlatter, B. Schneider, Y.M. Wright, K. Boulouchos, N-heptane micro pilot assisted methane combustion in a rapid compression expansion machine, Fuel, 179 (2016) 339-352.
7. A. Srna, M. Bolla, Y.M. Wright, K. Herrmann, R. Bombach, S.S. Pandurangi, K. Boulouchos, G. Bruneaux, Effect of methane on pilot-fuel auto-ignition in dual-fuel engines, Proc. Combust. Inst. 37 (4) (2019) 4741-4749.
8. M. Grochowina, D. Hertel, S. Tartsch, T. Sattelmayer, Ignition of diesel pilot fuel in dual-fuel engines, J. Eng. Gas Turbines Power 141 (8) (2019) 081021.
9. Z. Ahmad, O. Kaario, C. Qiang, V.Vuorinen, M. Larmi, A parametric investigation of diesel/methane

dual-fuel combustion progression/stages in a heavy-duty optical engine, Appl. Energy 251 (2019) 113191.

10. R.N. Dahms, G.A. Paczko, S.A. Skeen, L.M. Pickett, Understanding the ignition mechanism of high-pressure spray flames, Proc. Combust. Inst. 36 (2) (2017) 2615-2623.
11. S.A. Skeen, J. Manin, L.M. Pickett, Simultaneous formaldehyde PLIF and high-speed schlieren imaging for ignition visualization in high-pressure spray flames, Proc. Combust. Inst. 35 (3) (2015) 3167-3174.
12. J. O'Connor, M.P.B. Musculus, Effects of exhaust gas recirculation and load on soot in a heavy-duty optical diesel engine with close-coupled post injections for high-efficiency combustion phasing, Int. J. Engine Res. 15 (4) (2013) 421-443.
13. S.L. Kokjohn, M.P.B. Musculus, R.D. Reitz, Evaluating temperature and fuel stratification for heat-release rate control in a reactivity-controlled compression-ignition engine using optical diagnostics and chemical kinetics modeling, Combust. Flame 162 (6) (2015) 2729-2742.
14. L.M. Pickett, D.L. Siebers, C.A. Idicheria, Relationship between ignition processes and the lift-off length of diesel fuel jets, SAE Technical Paper 2005-01-3843, 2005.
15. H. Anders, M. Christensen, B. Johansson, A. Franke, M. Richter, M. Alden, A study of the homogeneous charge compression ignition combustion process by chemiluminescence Imaging, SAE Technical Paper 1999-01-3680, 1999.
16. M. Mehl, W.J. Pitz, C.K. Westbrook, H.J. Curran., Kinetic modeling of gasoline surrogate components and mixtures under engine conditions, Proc. Combust. Inst. 33 (1) (2011) 193-200.
17. B.W. Knox, C.L. Genzale, Reduced-order numerical model for transient reacting diesel sprays with detailed kinetics, Int. J. Engine Res. 17 (3) (2015) 261-279.
18. L.M. Pickett, J.A. Caton, M.P.B. Musculus, A.E. Lutz, Evaluation of the equivalence ratio-temperature region of diesel soot precursor formation using a two-stage Lagrangian model, Int. J.

Engine Res. 7 (5) (2006) 349-370.

19. G. Lacaze, A. Misdariis, A. Ruiz, J.C. Oeflein, Analysis of high-pressure Diesel fuel injection processes using LES with real-fluid thermodynamics and transport, Proc. Combust. Inst. 35 (2) (2015) 1603-1611.
20. M.P.B. Musculus, K. Kattke, Entrainment waves in diesel jets, SAE Int. J. Engines, 2 (1) (2009) 1170 -1193.
21. M.P.B. Musculus, T. Lachaux, L.M. Pickett, C.A. Idicheria, End-of-injection over-mixing and unburned hydrocarbon emissions in Low-Temperature-Combustion Diesel Engines, SAE Technical Paper, 2007-01-0907, 2007.
22. E. Mastorakos, Ignition of turbulent non-premixed flames, Prog. Energy Combust. Sci. 35 (1) (2009) 57-97.
23. C.A. Idicheria, L.M. Pickett, Ignition, soot formation, and end-of-combustion transients in diesel combustion under high-EGR conditions, Int. J. Engine Res. 12 (4) (2011) 376-392.
24. J.M. Desantes, R. Payri, F.J. Salvador, A. Gil, Development and validation of a theoretical model for diesel spray penetration, Fuel, 85 (7), 910-917.
25. J.V. Pastor, J.J. Lopez, J.M. Garcia, J.M. Pastor, A 1D model for the description of mixing-controlled inert diesel sprays, Fuel, 87 (13-14) (2008) 2871-2885.